# Early growth response 2 regulates mouse cooperative behavior

**Ming Xiao** ( mingx@njmu.edu.cn )
Nanjing Medical University
**Yanli Zhang**
Nanjing Medical University
**Weixi Feng**
Nanjing Medical University
**Ze Wang**
Nanjing Medical University
**Tianqi Wang**
Nanjing Medical University
**Yingting Pang**
Nanjing Medical University
**Yuxi Jin**
Nanjing Medical University
**Ying Zou**
Nanjing Medical University
**Yan Chen**
Nanjing Medical University
**Qian Li**
Nanjing Medical University
**Huang Huang**
Nanjing Medical University
**Chengyu Sheng**
Nanjing Medical University

**Biological Sciences - Article**

**Keywords:** Social Cooperation, Cooperative Deficits, Resocialization, Myelin Maturation, Corticosterone Levels, Neuropsychiatric Disorders

**Posted Date:** December 2nd, 2020

**DOI:** https://doi.org/10.21203/rs.3.rs-105053/v1

**Version of Record:** A version of this preprint was published at Lab Animal on January 16th, 2023. See the published version at https://doi.org/10.1038/s41684-022-01090-0.

# Abstract

Social cooperation is essential to animals' physical health and psychological state. However, the underlying molecular and neurobiological mechanisms remain poorly understood. Here, we established a novel model for systematically evaluating the cooperative behavior of mice for the task of water reward. Using this paradigm, we characterized cooperative deficits in isolated juvenile mice and the corrective effect of resocialization. Mechanistically, we found that the transcription factor early growth response 2 (Egr2)-dependent myelin maturation in the medial prefrontal cortex is necessary for the development of mice's cooperative behavior. Additionally, corticosterone levels in the serum and medial prefrontal cortex were elevated in the isolated mice, potentially contributing to Egr2 expression reduction. This work suggests targeting Egr2 could be targeted for preventing and treating social isolation-related neuropsychiatric disorders in the future.


# Main Text

Social cooperation is a highly conserved and sophisticated behavior that exists from bacterial swarming, ants, bees, rodents, primates to humans[1]. Cooperation is crucial for social species to overcome tasks that a single individual cannot accomplish, and thus contributes to their physical health, survival, and reproduction[2,3]. Disruptions in social behaviors frequently occur in a variety of disorders in the central nervous system (CNS) including depression, autism, schizophrenia, bipolar disorder, obsessive-compulsive disorder, and Alzheimer's disease[4-8]. Recently, several studies investigated cooperative behavior in fish model species and rats with different types of reward tasks[9-12]. However, the detailed neurobiological and molecular mechanisms underlying cooperative behavior remain largely undetermined. Addressing these issues will help to further explore brain functions and find potential therapeutic strategies for isolation-related neuropsychiatric disorders.

### Establishing a paradigm for evaluating mice's cooperative ability

We first established a system in which two mice are induced to accomplish position tasks simultaneously to get water. The mouse was first trained individually to complete the task and then get the water as a reward (**Fig. 1b & Supplementary Video 1**). After 7 consecutive days of training, all mice mastered to use this device to drink water, as reflected by the declining to latter flattened curve for drinking latency, and the rising to latter flattened curves for drinking number and drinking time (**Fig. 1b**, **c**). Subsequently, two trained mice were put into one cage, where the two mice could get water only if they accomplished the tasks simultaneously, a behavior we consider best explained by cooperation (**Fig. 1d**, **Supplementary Video 2**). Through the 5-day testing period, there was a consistent reduction in co-drinking latency, and consistent increases in co-drinking number and accumulated drinking time each day (**Fig. 1e**). This behavioral improvement could not be explained by stochastic co-occurrence, which should predict flattened curves for the individually trained mice. Therefore, we concluded that our setup were able to detect cooperative behavior in mice.

## Early social isolation (SI) led to cooperation defect in juvenile mice

SI has detrimental effects on animals' cognitive functions, mental health, and social performance[13,14]. We wondered if the cooperative performance is also affected. The 3-week-old weanling mice were randomly divided into two groups: SI (1 mouse per cage) and group housing (GH, 5 littermates per cage). After 3 weeks of the above social treatments, mice were then subjected to cooperative behavior training and testing (**Fig. 1a**). In the training period, SI mice improved slower than GH group on the individual water-drinking task in the first 4 days, but they gradually caught up and showed no significant difference at the end of the training (Day 7) (**Fig. 1c**). In the subsequent testing period, however, SI mice displayed dramatically prolonged co-drinking latency, up to about 3 times that of GH mice; the co-drinking number, as well as the co-drinking time, was also drastically reduced (**Fig. 1e & Supplementary Video 3**). What's more, unlike in the training period, SI mice didn't finally "catch up" in the testing period; like GH mice, they did show some improvement through time, but the gaps between the two respective curves never narrowed (**Fig. 1e**). These suggested SI greatly damaged mice's cooperation performance. In other behavior tests, SI mice displayed impairments in spatial working memory and fear learning and memory, reduces in locomotion and exploration, and anxiety-like behaviors (**Fig. 1f-i**), which are consistent with previous studies from our group and others[13-15].

## Immediate resocialization rescued mice's cooperation defect caused by early SI

A natural question to the isolation-elicited impairment is whether it could be rescued by resocialization. Thus, we transferred the 6-week-old SI mice into cages containing age-matched GH mice. After 4 additional weeks, these GH-SI mice were trained and tested for their cooperative performance (**Fig. 2a**). In the training period, we found the performance of GH-SI mice fell in between GH and SI group, with the curves more adjacent to the GH ones in general (**Fig. 2b**); in the testing period, GH-SI mice behaved largely indifferent to GH mice, indicating the isolation-induced cooperation defect was almost completely restored by resocialization (**Fig. 2c**). Similarly, GH-SI mice displayed comparable performance to GH mice on spatial working memory, fear learning and memory, locomotion, exploration, and anxiety-like behaviors (**Extended Data Fig. 2**).

Myelination in the medial prefrontal cortex (mPFC) is a known important target of social isolation[16]. We sought to see whether myelin and synaptic development were affected by the social treatments. The electron microscopy (EM) analysis on the ~12-week-old SI mice revealed elevated g-ratio, the ratio of the inner to the outer diameter of the myelin sheath as a measurement of sheath thickness, and reduced heterochromatin proportion, indicating impaired myelin development. Resocialization restored the myelin sheath thinning and partially rescued the heterochromatin reduction (**Fig. 2d-f**). Similarly, the synaptic maturation state was also affected by SI and rescued by resocialization (**Fig. 2d & e**). Additionally, immunohistology and Western blot further confirmed the EM result, as reflected by the expression of the mature oligodendrocyte marker protein myelin basic protein (MBP), the presynaptic marker synaptophysin and the postsynaptic marker PSD-95. These demonstrated the effect of SI and resocialization on myelin and synaptic integrity (**Fig. 2h-m**).

## RNA sequencing (RNA-seq) identified Egr2 as a critical regulator for mice's cooperative behavior

To explore the molecular mechanism underlying SI and resocialization, we performed RNA-seq on mPFC samples from the ~7-week-old GH and SI mice. We identified 1265 differentially expressed genes (DEGs) that were enriched in 4 pathways: cognitive behavior, myelin development, synaptic development, and ion channels (**Extended Data Fig. 3a-b**). After validating the mostly affected DEGs with real-time PCR (qPCR) and western blot, we further checked whether their expression could be restored by resocialization (**Extended Data Fig. 3c-l)**. Finally, we got 3 candidate genes showing consistent reduction (in SI mice) and restoration (in GH-SI mice): early growth response 1 (Egr1), early growth response 2 (Egr2), and activity-regulated cytoskeleton-associated protein (Arc) (**Extended Data Fig. 3m-n**). Intriguingly, the promoter regions of both Arc and Egr1 are predicted to be potential binding sites for Egr2. We performed a dual-luciferase reporter experiment in 293 cells and validated Egr2 could transcriptionally upregulate Arc and Egr1 expression (**Extended Data Fig. 4**). Therefore, these results suggested Egr2, the known critical transcription factor for PNS myelination and also for hindbrain development[17,18], as a possible master mediator for the effect of SI and resocialization.

Next, we generated an AAV9 virus expressing a shRNA targeting Egr2 (AAV-Egr2-RNAi). The 3-week-old weanling mice received virus injection into the bilateral mPFC and then group-housed or raised individually for 3 additional weeks (**Fig. 3a**, **Extended Data Fig. 5a**, **c**, **e-f**). AAV-Egr2-RNAi mice did not show any abnormalities in the cooperation-training period (**Fig. 3b**). The mice's performance on spatial working memory, fear learning and memory, locomotion, exploration, and anxiety-like behaviors were also unchanged (**Extended Data Fig. 6**). These results indicated Egr2 deficiency did not dampen mice's learning or emotional performance. However, in the subsequent cooperation-testing period, GH-Egr2-RNAi mice performed significantly worse than the control GH-GFP mice (**Fig. 3c**). We continued to explore if enhancing Egr2 could reverse the detrimental effect of SI. Like the AAV-Egr2-RNAi mice, overexpressing Egr2 in SI mice (SI-AAV-Egr2) did not alter mice's performance in the cooperation-training period (**Extended Data Fig. 7a-b**, **5b**, **d**, **g-h**). In the subsequent testing period, however, the performance of SI-AAV-Egr2 mice were dramatically improved compared to SI-GFP mice, and to a level close to the control GH-GFP group (**Extended Data Fig. 7c**). Egr2 overexpression did not change mice's performance on spatial working memory, locomotion, and exploration behavior, but the mice displayed improved performance on fear learning and memory, and reduced anxiety-like behavior (**Extended Data Fig. 8)**. Therefore, both RNAi and overexpression results identified a critical role of Egr2 in regulating mice's cooperative behavior.

## Egr2 was required for mPFC myelination and the middle stage maturation of oligodendrocyte

Next, we found knocking down Egr2 led to mPFC myelin impairment, as reflected by elevated g-ratio, reduced heterochromatin proportion, and reduced MBP expression, by EM, immunohistology, and western blot analysis (**Fig. 3d-j**). However, we did not identify any significant synaptic changes in GH-Egr2-RNAi mice, despite Egr2 is indeed expressed in mPFC neurons (**Extended Data Fig. 9**). In contrast to the RNAi results, overexpressing Egr2 in SI mice rescued both myelin and synaptic defect (**Extended Data Fig. 7d-**

**m**). This synaptic improvement was possibly a dosage effect of Egr2: overexpression of Egr2 could improve synaptic function through upregulation of Arc, although synaptic development normally does not require Egr2. Indeed, we performed chromatin immunoprecipitation (ChIP) coupled with qPCR (ChIP-qPCR) experiment and identified a strong binding of Egr2 with the 1700-1850bp region upstream of Arc's transcription initiation site (**Extended Data Fig. 10**).

Egr2 is an established master regulator for PNS myelination, where it promotes the late-stage Schwann cell maturation[19]. To see if Egr2 behaves similarly in the CNS oligodendrocytes, we knocked down Egr2 in the differentiating primary oligodendrocyte progenitor cells (OPCs). We found lack of Egr2 did not alter the expression of the early-stage marker platelet-derived growth factor alpha receptor (PDGFRα), but significantly reduced the middle stage marker ectonucleotide pyrophosphatase/phosphodiesterase 6 (Enpp6) and the late-stage marker MBP (**Fig. 3k-m, Extended Data Fig. 11**). Together, these results suggest Egr2 is required for mPFC myelination through promoting the middle-stage maturation of oligodendrocytes, but dispensable for neuronal synaptic development.

### Elevated corticosteroid production in SI mice may inhibit Egr2 expression

We continued to explore how mPFC Egr2 is regulated by the social treatments. As a kind of stress, early SI could stimulate the production of corticosteroid in the adrenal cortex in juvenile mice[20]. Corticosteroid treatment, on the other hand, is reported to inhibit oligodendrocyte proliferation, in sharp contrast to Egr2's promoting role[21]. Is it the elevated corticosteroid level suppresses Egr2 expression in SI mice? On mouse brain slices, immunofluorescence validated the existence of corticosteroid receptor (GR) and phosphorylated GR (pGR) in O4-expressing mPFC oligodendrocytes (**Fig. 4a-c**). For the mice receiving 3-week SI treatment, from the second week we evidenced a significant increase of the serum corticosteroid level (**Fig. 4d**). Additionally, we found a clear reverse correlation between a mouse's serum corticosteroid level and its mPFC Egr2 protein level (**Fig. 4e-f**). Treating primary oligodendrocytes with corticosteroid reduced Egr2 mRNA and protein expression (**Fig. 4g-i**). Therefore, our data suggest the elevated corticosteroid level in SI mice could lead to reduced Egr2 expression.

Taken together, as illustrated in **Fig. 4j**, we designed a new paradigm that could reliably and quantitatively evaluate mice's cooperative behavior. With this system, we found early SI led to cooperation defect that could be reversed by immediately followed resocialization; the myelination state and synaptic integrity in the mPFC are two main targets of SI and resocialization. We further identified the transcriptional regulator Egr2 conveys a major part of the effect of SI and resocialization on social cooperation. Egr2 works through promoting oligodendrocyte maturation, suggesting drugs targeting Egr2 or mPFC myelination could be explored for future preventing and treating of isolation-related neuropsychiatric disorders.

# Discussion

Rodents are prosocial animals and known to cooperate with one another. A few studies investigated the ability of rats to work together to obtain water or food[9,11]. However, these behavior paradigms are

relatively simple, and to some extent, not enough to reflect the characteristics of mutual adaptation and improvement in cooperative behavior. In this study, we investigated the cooperative behavior of mice in a long-term and multi-dimensional way following training them to learn to use a new device for drinking water. The results suggested that the behavior paradigm can well reflect the cooperative willingness (co-drinking latency) and efficiency (number and duration of co-drinking behavior) of mice. Through the testing period, their cooperative ability is continuously enhanced with the mutual benefit of getting more water. This is clear evidence that mice have remarkable social intelligence and mutual assistance skills.

The current results show juvenile SI mice have multiple behavioral abnormalities that are rescuable by resocialization. Correspondingly, the pathological evidence reveals that resocialization greatly attenuates myelin sheath and synaptic damages in the mPFC, which is consistent with previous reports[16,22]. Moreover, we demonstrated these isolated mice have impaired cooperative ability, which can be recovered with reintroduction into a social environment. Mechanistically, our results suggest the increased serum corticosteroid level results in the downregulation of Egr2 expression in the mPFC of the juvenile SI mice. Local overexpression of Egr2 can markedly mitigate the pathological defect in the mPFC and rescue the cooperative abnormalities in SI mice. Resocialization has corrective effects on multiple behaviors for SI mice, suggesting that besides the mPFC, it might also attenuate pathological damages of other brain regions. However, reducing Egr2 expression in the mPFC affects social cooperation specifically, without changing spatial working memory, fear learning and memory, locomotion, exploration, and anxiety-like behaviors. This may be attributed to the fact that mPFC is mainly responsible for controlling social behavior rather than emotion or working memory.

Egr2 has been shown to control Schwann cell myelination by modulating the expression of genes encoding myelin proteins and enzymes required for the synthesis of myelin lipids[23-25]. It also controls Schwann cell proliferation, differentiation, and death *in vitro*[19,26,27]. In the brain, Egr2 expression is induced under conditions like electroconvulsive shock, focal cerebral ischemia, opiate withdrawal, and limbic seizures[28-30]. Egr2 is also shown to play a key role in the stabilization of dentate gyrus long-term potentiation in adult mice[31]. In the present study, we have identified a crucial role of Egr2 in maintaining mPFC myelin and synapse integrity, which will advance our understanding of the neurobiological and molecular bases for mouse social cooperative behavior. However, Egr2 expresses in various brain regions including the neocortex, hippocampus, amygdala, olfactory bulb, striatum, cerebellum, diencephalic, and brainstem structures[28,32]. Whether there is a brain region-specificity role for Egr2 in brain functions needs to be clarified. Indeed, a recent study reported that the neuropeptide Tac2 coordinates complex behavioral effects after chronic SI tress in a distributed manner[33]. Whether Egr2 regulates different behavioral effects of SI in different brain regions in a similar way is worth exploring.

# References

1 Yan, J., Monaco, H. & Xavier, J. B. The Ultimate Guide to Bacterial Swarming: An Experimental Model to Study the Evolution of Cooperative Behavior. *Annu Rev Microbiol* **73**, 293-312 (2019).

2 Cacioppo, S., Balogh, S. & Cacioppo, J. T. Implicit attention to negative social, in contrast to nonsocial, words in the Stroop task differs between individuals high and low in loneliness: Evidence from event-related brain microstates. *Cortex* **70**, 213-233 (2015).

3 Holt-Lunstad, J. Why Social Relationships Are Important for Physical Health: A Systems Approach to Understanding and Modifying Risk and Protection. *Annu Rev Psychol* **69**, 437-458 (2018).

4 Kanter, J. W., Manos, R. C., Busch, A. M. & Rusch, L. C. Making behavioral activation more behavioral. *Behav Modif* **32**, 780-803 (2008).

5 Lai, M. C., Lombardo, M. V. & Baron-Cohen, S. Autism. *Lancet* **383**, 896-910 (2014).

6 Lahera, G. *et al.* Hostile attributions in bipolar disorder and schizophrenia contribute to poor social functioning. *Acta Psychiatr Scand* **131**, 472-482 (2015).

7 Mavrogiorgou, P. *et al.* Social cognition and metacognition in obsessive-compulsive disorder: an explorative pilot study. *Eur Arch Psychiatry Clin Neurosci* **266**, 209-216 (2016).

8 Porcelli, S. *et al.* Social brain, social dysfunction and social withdrawal. *Neurosci Biobehav Rev* **97**, 10-33 (2019).

9 Hernandez-Lallement, J., van Wingerden, M., Marx, C., Srejic, M. & Kalenscher, T. Rats prefer mutual rewards in a prosocial choice task. *Front Neurosci* **8**, 443 (2014).

10 Conde-Moro, A. R., Rocha-Almeida, F., Sanchez-Campusano, R., Delgado-Garcia, J. M. & Gruart, A. The activity of the prelimbic cortex in rats is enhanced during the cooperative acquisition of an instrumental learning task. *Prog Neurobiol* **183** (2019).

11 Marquez, C., Rennie, S. M., Costa, D. F. & Moita, M. A. Prosocial Choice in Rats Depends on Food-Seeking Behavior Displayed by Recipients. *Curr Biol* **25**, 1736-1745 (2015).

12 Soares, M. C., Cardoso, S. C., Carvalho, T. D. & Maximino, C. Using model fish to study the biological mechanisms of cooperative behaviour: A future for translational research concerning social anxiety disorders? *Prog Neuro-Psychoph* **82**, 205-215 (2018).

13 Skelly, M. J., Chappell, A. E., Carter, E. & Weiner, J. L. Adolescent social isolation increases anxiety-like behavior and ethanol intake and impairs fear extinction in adulthood: Possible role of disrupted noradrenergic signaling. *Neuropharmacology* **97**, 149-159 (2015).

14 Quan, M. N., Tian, Y. T., Xu, K. H., Zhang, T. & Yang, Z. Post weaning social isolation influences spatial cognition, prefrontal cortical synaptic plasticity and hippocampal potassium ion channels in

Wistar rats. *Neuroscience* **169**, 214-222 (2010).

15 Cao, M. *et al.* Early enriched physical environment reverses impairments of the hippocampus, but not medial prefrontal cortex, of socially-isolated mice. *Brain Behav Immun* **64**, 232-243 (2017).

16 Makinodan, M., Rosen, K. M., Ito, S. & Corfas, G. A critical period for social experience-dependent oligodendrocyte maturation and myelination. *Science* **337**, 1357-1360 (2012).

17 Jang, S. W., LeBlanc, S. E., Roopra, A., Wrabetz, L. & Svaren, J. In vivo detection of Egr2 binding to target genes during peripheral nerve myelination. *J Neurochem* **98**, 1678-1687 (2006).

18 De, S. & Turman, J. E., Jr. Krox-20 gene expression: influencing hindbrain-craniofacial developmental interactions. *Arch Histol Cytol* **68**, 227-234 (2005).

19 Tammia, M. *et al.* Egr2 overexpression in Schwann cells increases myelination frequency in vitro. *Heliyon* **4**, e00982 (2018).

20 Kim, J. S. & Iremonger, K. J. Temporally Tuned Corticosteroid Feedback Regulation of the Stress Axis. *Trends Endocrinol Metab* **30**, 783-792 (2019).

21 Wennstrom, M., Hellsten, J., Ekstrand, J., Lindgren, H. & Tingstrom, A. Corticosterone-induced inhibition of gliogenesis in rat hippocampus is counteracted by electroconvulsive seizures. *Biol Psychiat* **59**, 178-186 (2006).

22 Liu, J. *et al.* Impaired adult myelination in the prefrontal cortex of socially isolated mice. *Nat Neurosci* **15**, 1621-1623 (2012).

23 Jang, S. W. *et al.* Locus-wide identification of Egr2/Krox20 regulatory targets in myelin genes. *Journal of Neurochemistry* **115**, 1409-1420 (2010).

24 Martinez-Moreno, M. *et al.* Regulation of Peripheral Myelination through Transcriptional Buffering of Egr2 by an Antisense Long Non-coding RNA. *Cell Rep* **20**, 1950-1963 (2017).

25 Nagarajan, R. *et al.* EGR2 mutations in inherited neuropathies dominant-negatively inhibit myelin gene expression. *Neuron* **30**, 355-368 (2001).

26 Parkinson, D. B. *et al.* Krox-20 inhibits Jun-NH(2)-terminal kinase/c-Jun to control Schwann cell proliferation and death. *J Cell Biol* **164**, 385-394 (2004).

27 Hossain, S., de la Cruz-Morcillo, M. A., Sanchez-Prieto, R. & Almazan, G. Mitogen-activated protein kinase p38 regulates Krox-20 to direct Schwann cell differentiation and peripheral myelination. *Glia* **60**, 1130-1144 (2012).

28 Bhat, R. V., Worley, P. F., Cole, A. J. & Baraban, J. M. Activation of the zinc finger encoding gene krox-20 in adult rat brain: comparison with zif268. *Brain Res Mol Brain Res* **13**, 263-266 (1992).

29 An, G., Lin, T. N., Liu, J. S. & Hsu, C. Y. Induction of Krox-20 expression after focal cerebral ischemia. *Biochem Biophys Res Commun* **188**, 1104-1110 (1992).

30 Gass, P., Herdegen, T., Bravo, R. & Kiessling, M. High induction threshold for transcription factor KROX-20 in the rat brain: partial co-expression with heat shock protein 70 following limbic seizures. *Brain Res Mol Brain Res* **23**, 292-298 (1994).

31 Williams, J. *et al.* Krox20 may play a key role in the stabilization of long-term potentiation. *Brain Res Mol Brain Res* **28**, 87-93 (1995).

32 Beckmann, A. M., Davidson, M. S., Goodenough, S. & Wilce, P. A. Differential expression of Egr-1-like DNA-binding activities in the naive rat brain and after excitatory stimulation. *J Neurochem* **69**, 2227-2237 (1997).

33 Zelikowsky, M. *et al.* The Neuropeptide Tac2 Controls a Distributed Brain State Induced by Chronic Social Isolation Stress. *Cell* **173**, 1265-1279 e1219 (2018).

# Methods

### Animals and experimental treatment

Weanling male C57BL/6J mice (3-week-old) were randomly divided into GH and SI group. Five mice (for GH group) or a single mouse (for SI group) were housed in a plexiglass cage (31 cm × 22 cm ×15 cm) for 3 weeks as the social treatments (**Fig. 1a**); for resocialization, two SI mice were then put in a cage containing three GH mice for 4 weeks (**Fig. 2a**). For virus injection, 3-week-old weanling mice were injected with indicated viruses (AAV-Egr2-eGFP/AAV-Egr2-RNAi-eGFP or AAV-Control-eGFP) in the mPFC and then underwent the social treatments (**Fig. 3a**, **Extended Data Fig. 7a**). Mice were maintained on a 12-h light/dark cycle with ambient temperature (18-22°C) and humidity (30-50%), and having free access to food and water. All experiments were conducted in accordance with international standards on animal welfare and the guidelines of the Institute for Laboratory Animal Research of Nanjing Medical University.

### Behavioral test

Mouse activity in the following behavioral test was collected using a computer-connected digital video camera (TopScan, CleverSys, Inc., Reston, VA). Room lights, except for a dim light, were switched off during each experimental session for mouse comfort. Before each test, the apparatuses were cleaned with 70% alcohol to eliminate possible remaining olfactory cues. All tests were performed by two independent experimenters, who were each blind to the treatment schedule.

#### *Cooperative test*

The cooperative ability of mice was evaluated by a cooperative drinking device developed by our laboratory (**Fig. 1b-c**, **Supplemental video 1**). The device was plexiglass cage (60 cm × 40 cm × 35 cm) equipped with two water valves from which drop shape water could be delivered by turning on two serial photoelectric switches. During the first phase of training, named the training period, one photoelectric switch was defaulted ON; a mouse was placed into the chamber, and, in a 5-min period, it can explore and turn on the other switch to get water-rewards. Training was conducted over 7 consecutive days, with 2 trials per day. The latency for the first successful drinking, as well as the times and time of drinking during each trial were collected. During the second phase, named the testing period, both switches were defaulted OFF. Two trained mice were placed in the chamber and allowed to move freely for 10 min. Only if they turn on both switches at the same time, they can get the water-reward together. The co-drinking latency, times and time of co-drinking were recorded. The test was carried out once a day for five days. The mice were returned to their cages after each trail. To motivate mice to drink from the device, water supply was suspended for six hours before each trial. To increase their incentive for getting drinking water during the training or testing period, we made water unavailable from 6 hours before each training or testing; this short-term water deprivation had no significant effect on mice's exploratory activities, anxiety-like behavior, spatial working memory, or weight (**Extended Data Fig. 1**).

### *Open-field test*

The open field test was used to evaluate the locomotion and anxiety-like behaviors[34]. The open field consisted of a square blue box (60 cm × 60 cm × 25 cm), with an outlined center area (30 cm × 30 cm). Each mouse was placed in the center of box and allowed to move freely for 5 min within the box. The time spent in the center area, times of entering the center area and total distance traveled were calculated during the test.

### *Elevated plus maze test*

The anxiety-like behavior was also evaluated by the elevated plus maze that was composed of four arms (50 cm ×10 cm) connected by a central square (10 cm × 10 cm) and elevated 100 cm above the floor[15]. Two opposite arms were open, while the remaining were closed with 40 cm high walls. The mice were placed into the close arm and allowed to freely explore the maze for 5 min. The percentage of time spent and the frequency of entries into the open arm were calculated.

### *Y-maze test*

The spatial working memory of mice was examined using a Y-shaped maze[15]. The maze consisted of three arms (8× 30× 15 cm), with an angle of 120 degrees between each arm. The procedure included 5 min-training stage and 5 min-testing stage, with an interval of 2 h. During the first stage, one arm named novel arm (NA) was blocked by a baffle, allowing the mice to move freely in the other two arms for 5 min. During the second stage, the NA was opened and mice could freely explore throughout all 3 arms for 5 min. The percentage of time traveled in the NA arm, number of entries into the NA arm were analyzed.

### *Fear conditioning test*

The mouse was placed in the conditioning chamber for 3 min as a habituation period followed by one tone-foot-shock (tone, 30 s, 70 dB, 1 kHz; foot-shock, 2 s, 0.8 mA)[35]. The stimulation was given every two min within six min. The mouse was placed in the chamber again with tone-shock pairing (tone, 30 s, 70 dB, 1kHz) for 3 min after 24 h. Freezing behavior, defined as the absence of all visible movement of the body except the movement necessitated by respiration, was scored.

### RNA sequencing

Total RNA from the mPFC was extracted with RNAiso Plus (Takara, #9109) according to the manufacturer's instructions. The RNA quality and quantity were measured using NanoDrop 2000 (Thermo Scientific). RNA library was constructed using the BGISEQ-500 platform according to the manufacturer's instruction; after that, adapters were ligated to each end of the RNAs and subsequently reverse transcribed to create single-stranded cDNA and sequenced on the BGISEQ-500 platform with a read length of 50 bps. Stringent criteria were set to determine significantly dysregulated genes: adjusted p value below 0.05 and log2FC of greater than 1. The mPFC samples from SI and GH mice were analyzed as two independent datasets. Heatmaps representing z-scores were generated using the seaborn package in python.

### Plasmids and Adeno-associated virus

Egr2 and the scrambled control siRNA were purchased from RiboBio (Guangzhou, China) (**Supplemental Fig. 5i-j**). Egr2 overexpression plasmid, pcDNA3.1 vector, PGL3-basic vector, Arc luciferase reporter plasmid were obtained from GenScript (Nanjing, China). Adeno-associated viruses (AAV9s) for Egr2 overexpression (AAV-Egr2) or RNAi (AAV-Egr2-RNAi), and the control AAV-GFP virus were purchased from Genechem (Shanghai, China).

### Stereotaxic injection

Deeply anesthetized mice were fixed in a stereotaxic instrument with the skull surface exposed. A total of 1.5 µl of AAV-Egr2, AAV-Egr2-RNAi ($1 \times 10^{13}$ µg) or control virus (AAV-GFP) were infused bilaterally into the mPFC at the following coordinates: +1.5 mm anterior/posterior, -0.75 mm dorsal/ventral and ±1.0 mm medial/lateral relative to Bregma use 33-gauge syringe needles (Hamilton)[36]. The infusion rate was 0.2 µl/min, and the cannula was left in the place for 5 min following completion of the infusion. Mice were allowed to recover for 2 days before isolated housing. Behavioral experiments were performed 21 days after the injection. Following the behavioral tests, mice were perfused and brain sections were examined by electron microscopy, qPCR, histology, or Western blot analysis.

### Primary OPCs culture and differentiation

The cortices from postnatal 5-7-day old C57Bl/6J mouse pups were quickly dissected and diced with a scissors after removing the meninges and blood vessels. Tissue was digested in Neurobasal (Thermo

Fisher, #21103049) with 20-30 U/ml Papain (Sangon Biotech, #A003124-0100) and 2500 U DNase I (Sigma, #D4513) at 37°C for 20 min; the digested cells were pelleted and resuspended in Neurobasal with 2% B27 (Gibco Thermo Fisher, 17504044), and then filtered through a 40 μm mesh filter (BD Falcon, #352340); the filtered cells were pelleted and resuspended again in PBS containing anti-O4 beads (Miltenyi Biotec, #130-094-543): 90 μl PBS and 10 μl beads per $1\times10^7$ cells; cells and beads were incubated at 4°C for 15 min, with the tube finger-tapped 4-5 times every 5 min; a column (Miltenyi Biotec, #130-042-201) was then used to capture the beads and thus enrich the O4-positive primary OPCs; the OPCs were resuspended in the proliferation medium consisted of DMEM-F12 (Thermo Fisher, #11320-033) with 1% N2 (Gibco thermofisher, #17502-048), 2% B27, 1% penicillin/streptomycin (Gibco Thermofisher, #15140-122), and 40 ng/ml PDGF-AA (R&D Systems, #1055-AA-050), and plated onto 24-well or 6-well plate covered with PDL (sigma, #P6407) and laminin (Sigma, #114956-81-9) at a density of 9000-15000 cells/$cm^2$. The proliferation media was replaced completely by fresh one on the first day, and then half changed every other day. After 8-9 days of proliferation, the medium was replaced by the differentiation medium that is consisted of DMEM-F12 with 1% N2, 2% B27, 1% penicillin/streptomycin, 50 μg/ml insulin (sigma, #I-6634), 40 ng/ml triiodo tyrosine (Sigma, #T2877), and 1 ng/ml ciliary neurotrophic factor (R&D Systems, #557-NT) to differentiate oligodendrocyte.

## Cell lines

Neuro-2a cell was a gift from Dr. Gang Hu (Nanjing Medical University) and was used for the ChIP, luciferase reporter assay and western blot analysis. For transfection, the cells were plated 24 hours before and then transfected with appropriate constructs using Lipofectamine 2000 (Invitrogen, #52887) according to the manufacturer's instruction. Culture medium was replaced 5-6 hours after transfection; transfected cells were cultured for 24 additional hours for q-PCR or 48 h for Western blotting.

## Luciferase reporter assay

The luciferase reporter assay for Arc/Egr1 promoter activity was performed according to the manufacturer's instructions (Promega, E1910). Briefly, 0.05 μg luciferase reporter plasmid, 0.2 μg EGR2 expression plasmid and 1.25 ng Renilla were co-transfected into the 80-90% confluence Neuro-2a cells; 48 hours after the transfection, cells were harvested and resuspended in 50 μl passive lysis buffer, and then placed on a micro oscillator and split for 15 min. The supernatant was used to measure luciferase activity; the normalized values (Renilla/firefly activity) were used for analysis. Experiments were performed in triplicate.

## ChIP and ChIP qPCR data analysis

We used a Magna ChIP Kit (Millipore, #17-10085) for the chromatin analysis. Briefly, Neuro-2a cells were cross-linked with 1% formaldehyde; the cells were collected by scratching, and then lysed and resuspended in nuclear buffer. 24 cycles of sonication (10 s for each, followed by a 20 s interval) were applied to break the chromatin into fragments between 200 and 1000 bp. The samples were incubated with anti-Egr2 antibody (Santa Cruz, #sc-293195) or anti-RNA polymerase antibody (Millipore, #17-

10085) and magnetic beads overnight at 4°C. Normal IgG was used as a negative control. The immunoprecipitants were separated by magnetic rack and washed. The DNA fragments were released by incubation with proteinase K at 62°C for 3 h with continuous shaking, and isolated by filtration. qPCR was performed in a 20-μl reaction volume using the SYBR Green PCR master mix (Takara, #RR420B). For electrophoresis analysis, PCR was performed with a NEB Next High-Fidelity 2X PCR Master Mix (New England Biolabs) with product resolved by agarose electrophoresis, followed by gel imaging. ChIP-qPCR (qChIP) primers were designed in proximity to Arc binding motif sequences. For each gene of interest, separate primer pairs were designed. The PCR primers are listed in (**Supplementary Table 1**). qChIP results were presented as percent to input.

### Corticosterone Assay

Orbit blood was collected from mice into ice-cooled centrifugal tubes and centrifuged (1700 ×g, 10 min, 4°C) to separate serum and stored below 80°C until the assay. Blood sampling took place between 09:00 and 12:00 h[37]. Corticosterone was quantified by the enzyme-linked immunosorbent assay (Parameter Corticosterone Assay R&D Systems, #KGE009) according to assay instructions. All samples were run in duplicate, counterbalanced across plates, and were within the standard curve. Final values were determined by averaging the results of duplicated samples.

### Immunohistochemistry and immunofluorescence.

Immunohistochemical staining was performed as previously described[38]. Briefly, cardiac of the anesthetized mice was poured into 0.9% saline by perfusion pump for 2 min, followed by 4% paraformaldehyde for 7 min. Brain tissue were post-fixed overnight in 4% PFA. For immunohistochemical staining, brain tissues were dehydrated in a series of graded ethanol solutions, embedded in paraffin and serially cut at 5-μm, using a paraffin slicing machine (Leica, Germany). Brain tissue sections containing the mPFC or hippocampus were incubated with a primary antibody anti- Synaptophysin (Millipore, #MAB5258-I, 1:100 dilution), anti-PSD-95 (abcam, #ab18258, 1:200 dilution) or anti-MBP (abcam, #ab7349, 1:200 dilution) at 4°C overnight. For immunofluorescence staining, brain tissues were cryoprotected overnight in 30% sucrose in phosphate buffer solution (PBS); the tissue was then embedded in OCT compound (SUKURA, #4583), and cut on a cryostat (Leica, Germany) at a thickness of 15 μm, mounted on super frost plus slides and stored at -20°C. For the staining, the sections were air dried for 1 hour at room temperature and rinsed with 1× PBS, blocked and permeabilized in blocking solution (2.5% bovine serum albumin in PBS) containing 0.1% Triton X for 1 hour at room temperature, incubated overnight at 4°C with primary antibodies anti-Tuj1 (santa cruz, #sc-80005, 1:200 dilution), anti-O4 (R&D, #MAB1326, 1:200 dilution), anti-MBP (abcam, #ab7349, 1:200 dilution), anti-EGR2 (Novus, #NB100-92327, 1:200 dilution), anti-GR (santa cruz, #sc-393232, 1:50 dilution) or anti-P-GR (Technology, #4161S, 1:200 dilution), and then with the corresponding fluorescent probe-conjugated secondary antibodies (Thermo Fisher, #A21202, #A21206, #A31572, #A31570 and #A31571) for 2 h at room temperature. For primary oligodendrocyte staining, fixed coverslips were incubated with primary antibodies anti-O4 (R&D, #MAB1326, 1:200 dilution), anti-MBP (abcam, #ab7349, 1:200 dilution) and anti-

Egr2 (Novus, # NB100-92327, 1:200 dilution). Nuclei were stained with 4, 6-diamidino-2-phenylindole (DAPI) at a 1:1000 dilution. Pictures were taken with an LSM700 confocal microscope (Zeiss, Germany).

### Electron microscopy

Cardiac of the anesthetized mice was poured into 0.9% saline by perfusion pump for 2 min, followed by 2.5% glutaraldehyde, 2% paraformaldehyde in 0.1 M PB. The brain was rapidly removed and post-fixed (4% paraformaldehyde and 2.5% glutaraldehyde in 0.1 M phosphate buffer containing 0.5% NaCl) for at least one week at 4°C. Following washing with distilled water, the sections were stained with 0.5% uranyl acetate in 70% ethanol for 1 h, dehydrated in a serial dilution of ethanol, and cleared in propylene oxide, embedded in Epon, and incubated at 60°C for 24 h. The tissues in Epon blocks were then trimmed and reoriented so that ultrathin (70 nm) cross sections were cut using the ultramicrotome (Leica EM UC7).

### Quantitative real-time PCR

Total RNA from the mPFC were extracted with TRIzol according to the manufacturer's instructions. cDNAs were synthesized from 1 μg total RNA using the Maxima First Strand Synthesis Kit for RT-qPCR (Takara, #RR047B). qPCR was performed by amplifying cDNA for 40 cycles using the SYBR Green PCR master mix. Relative expression of mRNA for the target genes was calculated by the comparative ΔΔCt method using GAPDH as control reference genes. The primers for Egr2, Myoc, Rxrg, Adora2a, Lef1, Drd1, Nab2, Rarb2, Dusp10, Cldn11, Arc, Nr4a2, Myo3b, Drd2, Egr1, Cd24a, Sdk2, NTs, Cartpt, Slc10A4, Drd5, Zic1, Htr1d, Pcsk9, Oligo2, Sox10, ErbB3, PDGFa, Enpp6, MBP, CC1 and GAPDH were synthesized by TsingKe (Beijing, China). All primer information is listed in (**Supplementary Table 3**). Six (for RNA extraction) or four (for qPCR) mice per group in duplicate experiments were averaged to provide a mean value for each group.

### Western blotting

For Western blot analyses, samples were lysed in the RIPA buffer (Beyotime, #P0013B) containing protease inhibitors (Beyotime, #st506) and phosphatase inhibitors (Roche, #04906837001). Cell lysates were cleared of cellular debris by centrifugation (12000 rpm for 15 min) and equal amounts of protein were loaded in the SDS-PAGE on 8-12% gels and transferred to PVDF membranes. After blocking for 1 h in 5% nonfat milk in TBST, the membranes were incubated at 4℃ overnight with one of the following primary antibodies: anti-Egr1 (santa cruz, #sc-189, 1:1000 dilution), anti-Egr2 (santa cruz, #sc-293195, 1:1000 dilution), anti-Arc (santa cruz, #sc-17839, 1:1000 dilution), anti-Lef1 (Proteintech, #14972-1-AP, 1:500 dilution), anti-Nab2 (Proteintech, #19601-1-AP, 1:1000 dilution), anti-NTs (Immunoway, #YT5535, 1:500 dilution), anti-Pcsk9 (Proteintech, #55206-1-AP, 1:500 dilution), anti-BDNF (abcam, #ab108319, 1:1000 dilution), anti-Trkb (santa cruz, #sc-12, 1:500 dilution), anti-Erk (Technology, #8201, 1:1000 dilution), anti-Slc10a4 (abcam, #ab107407, 1:500 dilution), anti-Htr1d (Novus, # NB100-56349SS, 1:250 dilution), anti-Synaptophysin (Millipore, #MAB5258-I, 1:1000 dilution), anti-PSD-95 (abcam, #ab18258, 1:1000 dilution), anti-MBP (abcam, #ab7349, 1:1000 dilution) and anti-GAPDH (Proteintech, #60004-1-Ig, 1:3000 dilution). HRP-conjugated secondary antibodies are from Vector Laboratories; bands were

visualized using ECL plus detection system (Imagequant LAS4000 mini). Quantification was performed using Gelpro32.

### Image analysis.

Light and electron micrographs were analyzed with the aid of Image J (NIH, USA). The mean integrated optical density was measured to assess immunostaining intensity of MBP, Synaptophysin, PSD-95 and Egr2 in the mPFC, respectively. Three sections per mouse, and four mice per group, were averaged to provide a mean value for each group. A minimum of 15 electron micrographs per animal, taken at 10000×, were collected from the layer II/III pyramidal neurons in the anterior cingulate of mPFC. These micrographs were used to determine the extent of heterochromatin of individual oligodendrocyte lineage cells. The total nuclear area of each cell was calculated, and heterochromatin was selected using the threshold tool and reported as percentage of total nuclear area. In addition, the *g* ratio that used for determination of the extent of myelination was calculated as the diameter of the axon divided by the diameter of the entire myelinated fiber as previously described[22]. A minimum of 100 myelinated axons per area of interest, per animal, were analyzed. The synaptic structure was analyzed by measuring the thickness of the postsynaptic dense, synaptic cleft width, length of the active zones, synaptic curvature. An average of 10 measurements of synaptic cleft width evenly spaced across the synapse was taken as a reading for each synapse, where the ends of the synapse were defined as the ends of the electron-dense PSD. The length of the active zones was measured, and synaptic curvature was subsequently calculated from the ratio of the arc length of the active zone to its corresponding chord length[39]. To avoid bias, images were analyzed by an individual who was blind to the experimental condition.

### Statistical analysis.

Statistical analysis was performed with Prism 6.0 (GraphPad Software). The number of animals and culture used for the experiments are indicated in the bar graphs of the Fig.s or in the Fig. legends. The cooperative training and cooperative test date were analyzed by repeated-measures ANOVA. The comparisons between two groups were examined by two-tailed Student's t-tests. The two-way ANOVA followed by Tukey's multiple comparisons test was performed for multiple groups. Data shown are the mean ± SEM. with $P < 0.05$ considered statistically significant.

34 Wang, L. *et al.* Deep cervical lymph node ligation aggravates AD-like pathology of APP/PS1 mice. *Brain Pathol* **29**, 176-192 (2019).

35 Gao, J. *et al.* A novel pathway regulates memory and plasticity via SIRT1 and miR-134. *Nature* **466**, 1105-1109 (2010).

36 Matos, M. R. *et al.* Memory strength gates the involvement of a CREB-dependent cortical fear engram in remote memory. *Nat Commun* **10**, 2315 (2019).

37 Kinn Rod, A. M., Harkestad, N., Jellestad, F. K. & Murison, R. Comparison of commercial ELISA assays for quantification of corticosterone in serum. *Sci Rep* **7**, 6748 (2017).

38 Xu, Z. *et al.* Deletion of aquaporin-4 in APP/PS1 mice exacerbates brain Abeta accumulation and memory deficits. *Mol Neurodegener* **10**, 58 (2015).

39 Jones, D. G. & Devon, R. M. An ultrastructural study into the effects of pentobarbitone on synaptic organization. *Brain Res* **147**, 47-63 (1978).

# Declarations

**Acknowledgements** We thank Dr. Lingqiang Zhu (Tongji Medical College of HUST) and Dr. Qigang Zhou (Nanjing Medical University) for their insightful comments and Mr. Zhengrong Xia for technical assistance with the electron microscopy. This work was supported by the grants from by the National Natural Science Foundation of China (81801378 and 81871117).

**Author Contributions** M.X., C.S., Y.Z., and W.F. designed the experiments. Y.Z. and W.F. performed most of the experiments and analysis, Y.Z., W.F., Z.W., T.W., Y.P., Y.J., Y.C., and L.Q. did the behavioral experiment. The manuscript was written by M.X., C.S., Y.Z. and W.F.. All authors discussed results, made Figures and edited the manuscript. M.X., C.S., and H.H. directed and supervised all aspects of the study.

**Data availability** All RNA-seq datasets are available at GEO (Accession codes are under application). The data that supports the finding of the study are available from the corresponding authors upon reasonable request.

# Figures

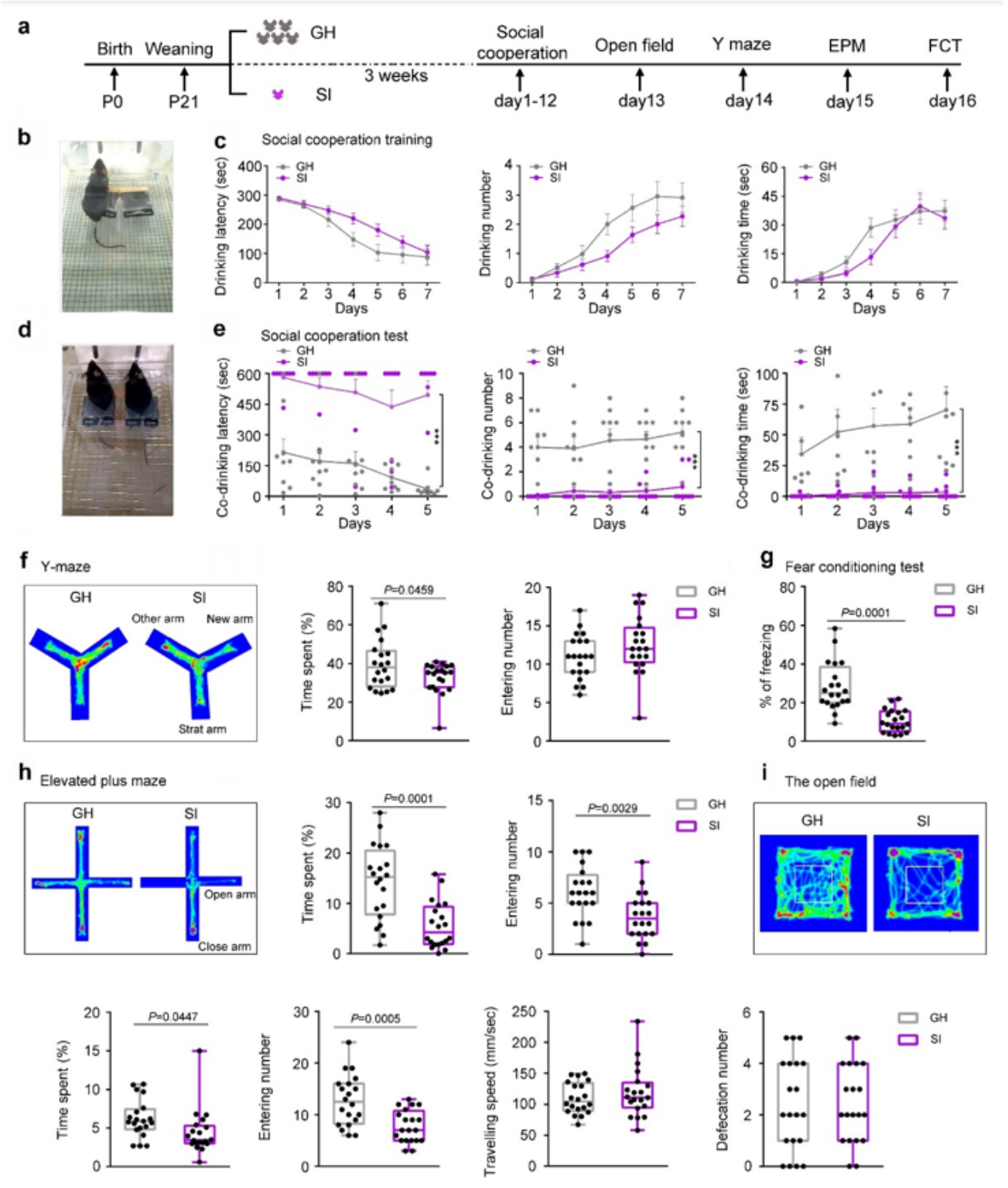


## Figure 1

Setup of a novel cooperative water-drinking system and identifying effect of SI on mice cooperation and other behaviors. a, A timeline diagram showing mice receiving weanling, social isolation, cooperative water-drinking test, and other behavioral tests. b, The training setup for the cooperative water-drinking experiment. c, Graphs showing the time before the first drinking (drinking latency), the times of drinking (drinking number), and the total time spent on drinking (drinking time) each day in the training period.

Note a successful training is reflected by the declining (or rising) to latter flattened curves. d, The testing setup for the cooperative water-drinking experiment. e, Graphs showing the cooperation performance in the testing setup for GH and SI mice. Note the separation of the two curves in each graph, as assessed by the elevated drinking latency ($F(1, 80) = 70.621$, $P = 0.0001$), reduced drinking number ($F(1, 80) = 104.823$, $P = 0.0001$), and reduced drinking time ($F(1, 80) = 130.235$, $P = 0.0001$). f, The spatial working memory performance of GH and SI mice in the Y-maze testing. g, Fear memory performance of GH and SI mice in fear conditioning test. h, The anxiety levels of GH and SI mice examined by the elevated plus maze test. i, Locomotion, and exploration behavior of GH and SI mice in the open field. All data were from 2 months old male C57BL/6 mice. Data in f-i, were analyzed by two-tailed Student's t-tests. n = 20 in each group; Data in c, e were analyzed by Repeated Measures ANOVA with post hoc Student-Newman-Keuls test and presented as mean ± SEM from 18 mice per group. Data were presented as line plot in c and with dots representing values of each sample in e, and as box plot with dots for f, i. GH: group housing; SI: social isolation.

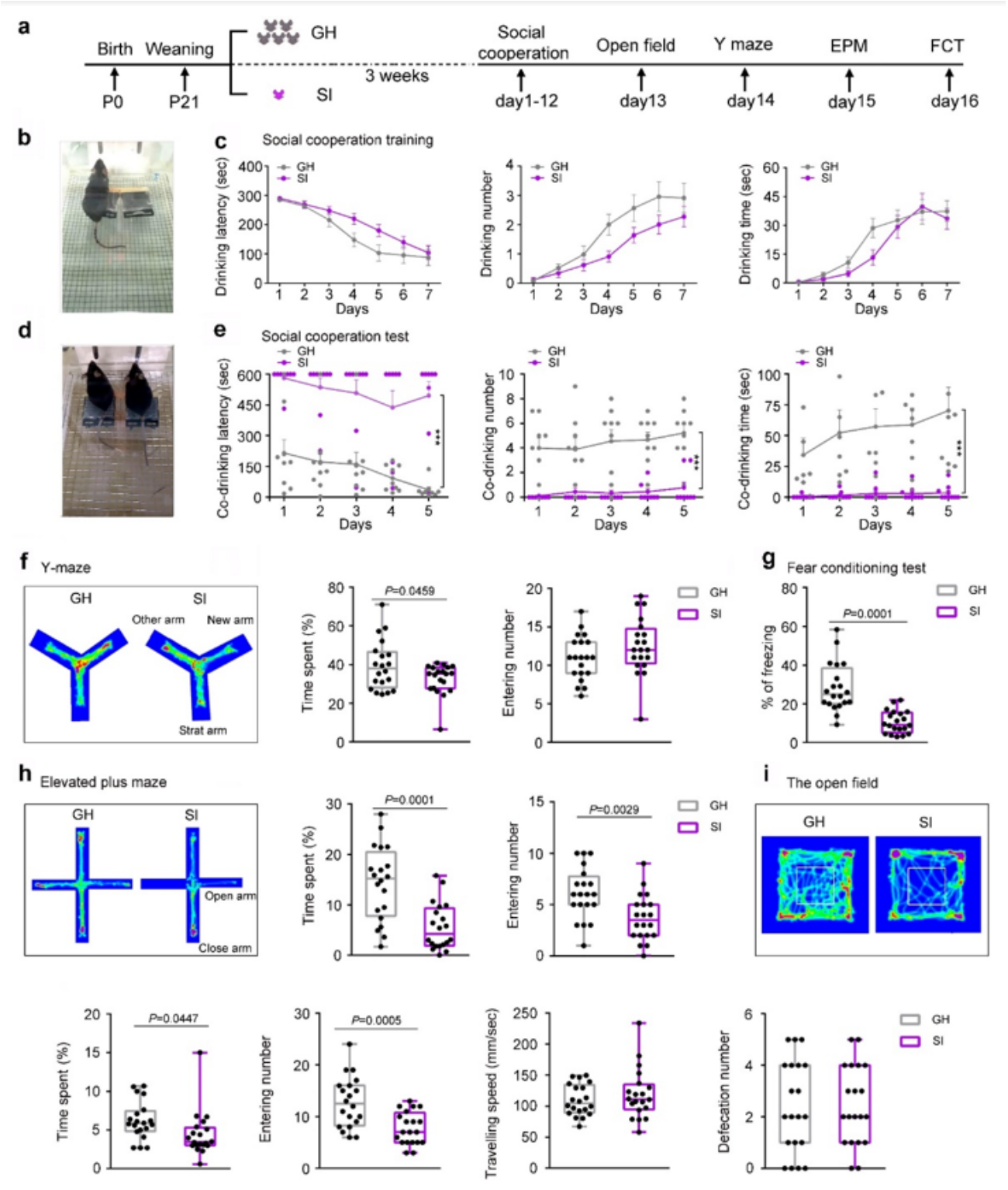


## Figure 1

Setup of a novel cooperative water-drinking system and identifying effect of SI on mice cooperation and other behaviors. a, A timeline diagram showing mice receiving weanling, social isolation, cooperative water-drinking test, and other behavioral tests. b, The training setup for the cooperative water-drinking experiment. c, Graphs showing the time before the first drinking (drinking latency), the times of drinking (drinking number), and the total time spent on drinking (drinking time) each day in the training period.

Note a successful training is reflected by the declining (or rising) to latter flattened curves. d, The testing setup for the cooperative water-drinking experiment. e, Graphs showing the cooperation performance in the testing setup for GH and SI mice. Note the separation of the two curves in each graph, as assessed by the elevated drinking latency ($F(1, 80) = 70.621$, $P = 0.0001$), reduced drinking number ($F(1, 80) = 104.823$, $P = 0.0001$), and reduced drinking time ($F(1, 80) = 130.235$, $P = 0.0001$). f, The spatial working memory performance of GH and SI mice in the Y-maze testing. g, Fear memory performance of GH and SI mice in fear conditioning test. h, The anxiety levels of GH and SI mice examined by the elevated plus maze test. i, Locomotion, and exploration behavior of GH and SI mice in the open field. All data were from 2 months old male C57BL/6 mice. Data in f-i, were analyzed by two-tailed Student's t-tests. n = 20 in each group; Data in c, e were analyzed by Repeated Measures ANOVA with post hoc Student-Newman-Keuls test and presented as mean ± SEM from 18 mice per group. Data were presented as line plot in c and with dots representing values of each sample in e, and as box plot with dots for f, i. GH: group housing; SI: social isolation.

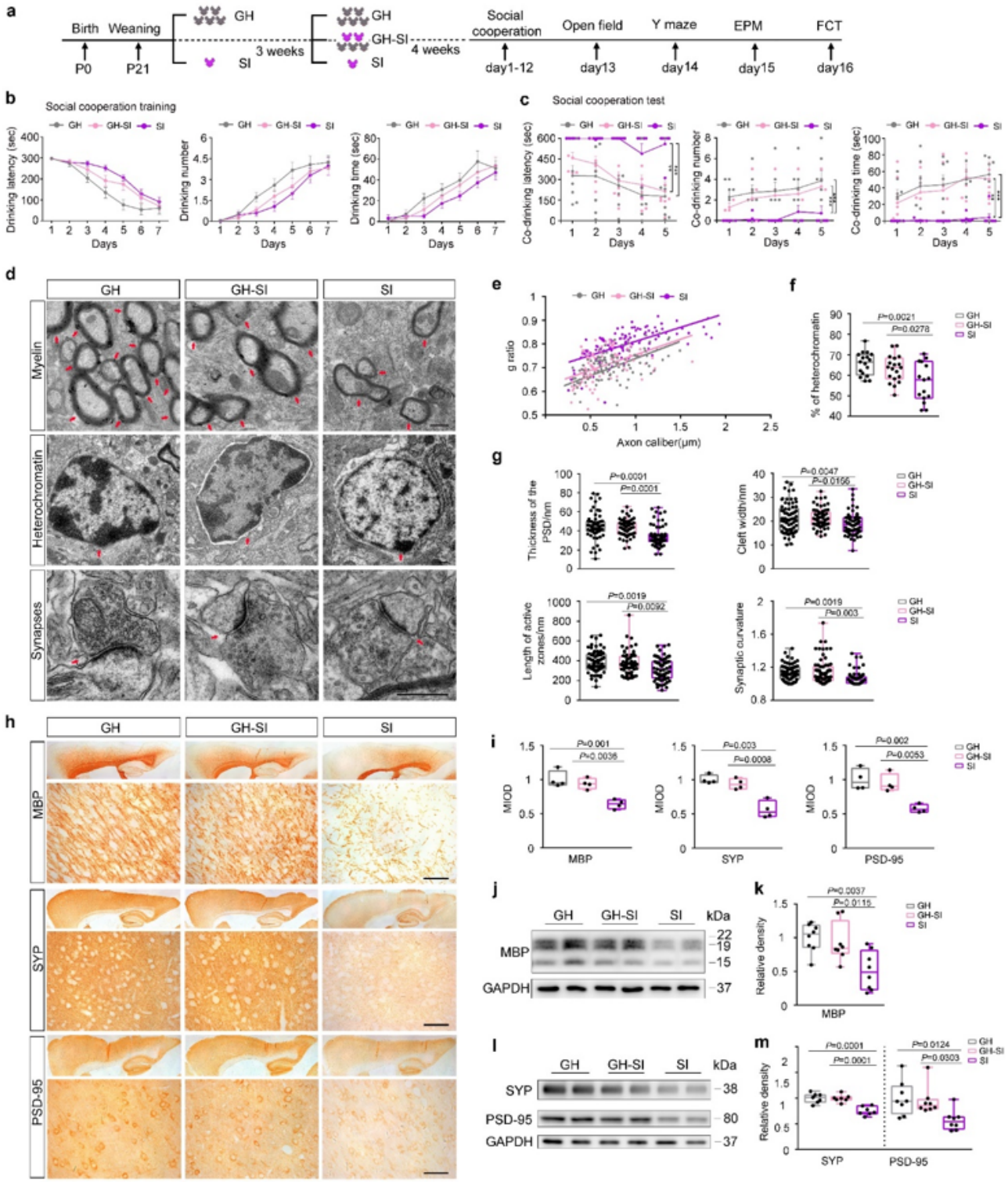


## Figure 2

The cooperation defect and mPFC impairment of SI mice were rescued by resocialization. a, A timeline diagram showing mice receiving weanling, social isolation, resocialization, cooperative water-drinking test, and other behavioral tests. b, c, Graphs showing the time before the first drinking (drinking latency), the times of drinking (drinking number), and the total time spent on drinking (drinking time) each day in the training (b) and testing (c) periods. Note curves of GH-SI mice are closer to GH ones in c. as assessed

by the elevated drinking latency ($F(1, 90) = 12.933$, $P = 0.0001$), reduced drinking number ($F(1, 90) = 17.267$, $P = 0.0001$), and reduced drinking time ($F(1, 90) = 11.907$, $P = 0.001$). d, Representative electron microscopy (EM) images showing mPFC myelin, heterochromatin, and synaptic morphology in GH, GH-SI and SI mice. Red arrows in each row indicate representative myelin (top), heterochromatins (middle), and synapses (bottom) respectively; scale bar, 500 nm. e-g, Graphs showing the quantified analysis of myelin (e), heterochromatin (f) and synaptic morphology (g). e, shows the scatter plots of g-ratios with linear least squares fitting (g-ratio vs. axon caliber); note GH-SI curve is closer to GH one; statistical significance was assessed by sum-of-squares F test of the slopes; n = 106, 107, and 110 axons for GH, GH-SI and SI group, respectively. f, shows the percentage of nuclear heterochromatin in GH, GH-SI and SI mice, n = 17, 19, and 15 respectively. g, shows postsynaptic density thickness, synaptic cleft width, presynaptic active zones length, and synaptic curvature in GH, GH-SI and SI mice, n = 70, 68, and 63 synapses respectively. h-m, Representative immunohistology (h) and western blot images (j, l,) showing MBP, Synaptophysin and PSD-95 expression in the mPFC of GH, GH-SI, and SI mice; correspondingly quantified analyses are shown in i (for h), k (for j), and m (for i); scale bar, 50 μm; All data were from 3 months old male C57BL/6 mice. n = 4 mice for h, n = 8 for j, l. Data were presented as mean ± SEM for b, c, e, f, g, i, k and m. Data in b, c were from 14 mice per group and analyzed by Repeated Measures ANOVA with post hoc Student-Newman-Keuls test. All comparisons were done by One-way ANOVA followed by Tukey's post hoc test; Data were presented as line plot in b and with dots representing values of each sample in c, and as box plot with dots for others. GH: group housing; SI: social isolation; GH-SI: resocialization of SI mice with GH mice.

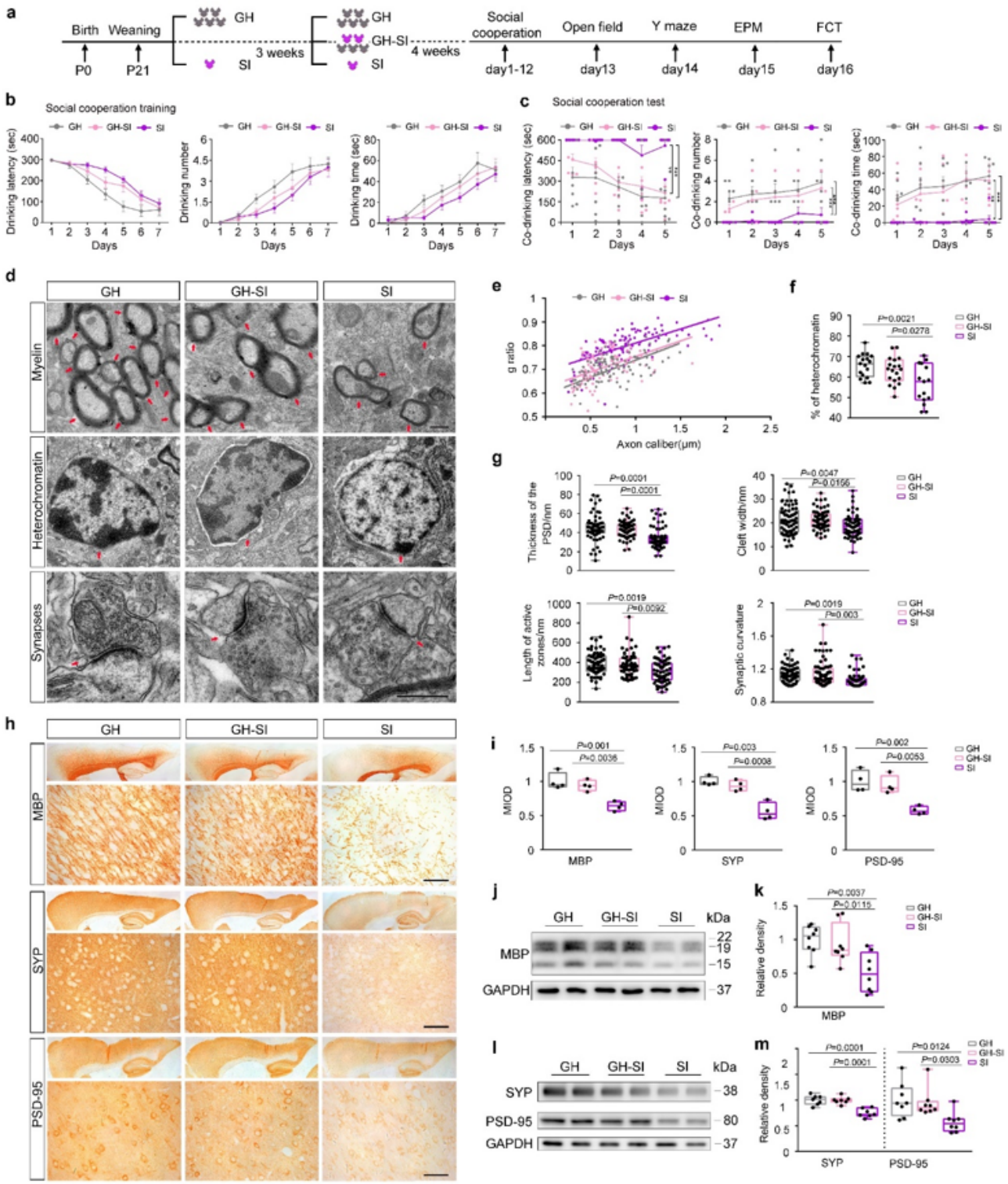


## Figure 2

The cooperation defect and mPFC impairment of SI mice were rescued by resocialization. a, A timeline diagram showing mice receiving weanling, social isolation, resocialization, cooperative water-drinking test, and other behavioral tests. b, c, Graphs showing the time before the first drinking (drinking latency), the times of drinking (drinking number), and the total time spent on drinking (drinking time) each day in the training (b) and testing (c) periods. Note curves of GH-SI mice are closer to GH ones in c. as assessed

by the elevated drinking latency ($F(1, 90) = 12.933$, $P = 0.0001$), reduced drinking number ($F(1, 90) = 17.267$, $P = 0.0001$), and reduced drinking time ($F(1, 90) = 11.907$, $P = 0.001$). d, Representative electron microscopy (EM) images showing mPFC myelin, heterochromatin, and synaptic morphology in GH, GH-SI and SI mice. Red arrows in each row indicate representative myelin (top), heterochromatins (middle), and synapses (bottom) respectively; scale bar, 500 nm. e-g, Graphs showing the quantified analysis of myelin (e), heterochromatin (f) and synaptic morphology (g). e, shows the scatter plots of g-ratios with linear least squares fitting (g-ratio vs. axon caliber); note GH-SI curve is closer to GH one; statistical significance was assessed by sum-of-squares F test of the slopes; n = 106, 107, and 110 axons for GH, GH-SI and SI group, respectively. f, shows the percentage of nuclear heterochromatin in GH, GH-SI and SI mice, n = 17, 19, and 15 respectively. g, shows postsynaptic density thickness, synaptic cleft width, presynaptic active zones length, and synaptic curvature in GH, GH-SI and SI mice, n = 70, 68, and 63 synapses respectively. h-m, Representative immunohistology (h) and western blot images (j, l,) showing MBP, Synaptophysin and PSD-95 expression in the mPFC of GH, GH-SI, and SI mice; correspondingly quantified analyses are shown in i (for h), k (for j), and m (for i); scale bar, 50 μm; All data were from 3 months old male C57BL/6 mice. n = 4 mice for h, n = 8 for j, l. Data were presented as mean ± SEM for b, c, e, f, g, i, k and m. Data in b, c were from 14 mice per group and analyzed by Repeated Measures ANOVA with post hoc Student-Newman-Keuls test. All comparisons were done by One-way ANOVA followed by Tukey's post hoc test; Data were presented as line plot in b and with dots representing values of each sample in c, and as box plot with dots for others. GH: group housing; SI: social isolation; GH-SI: resocialization of SI mice with GH mice.

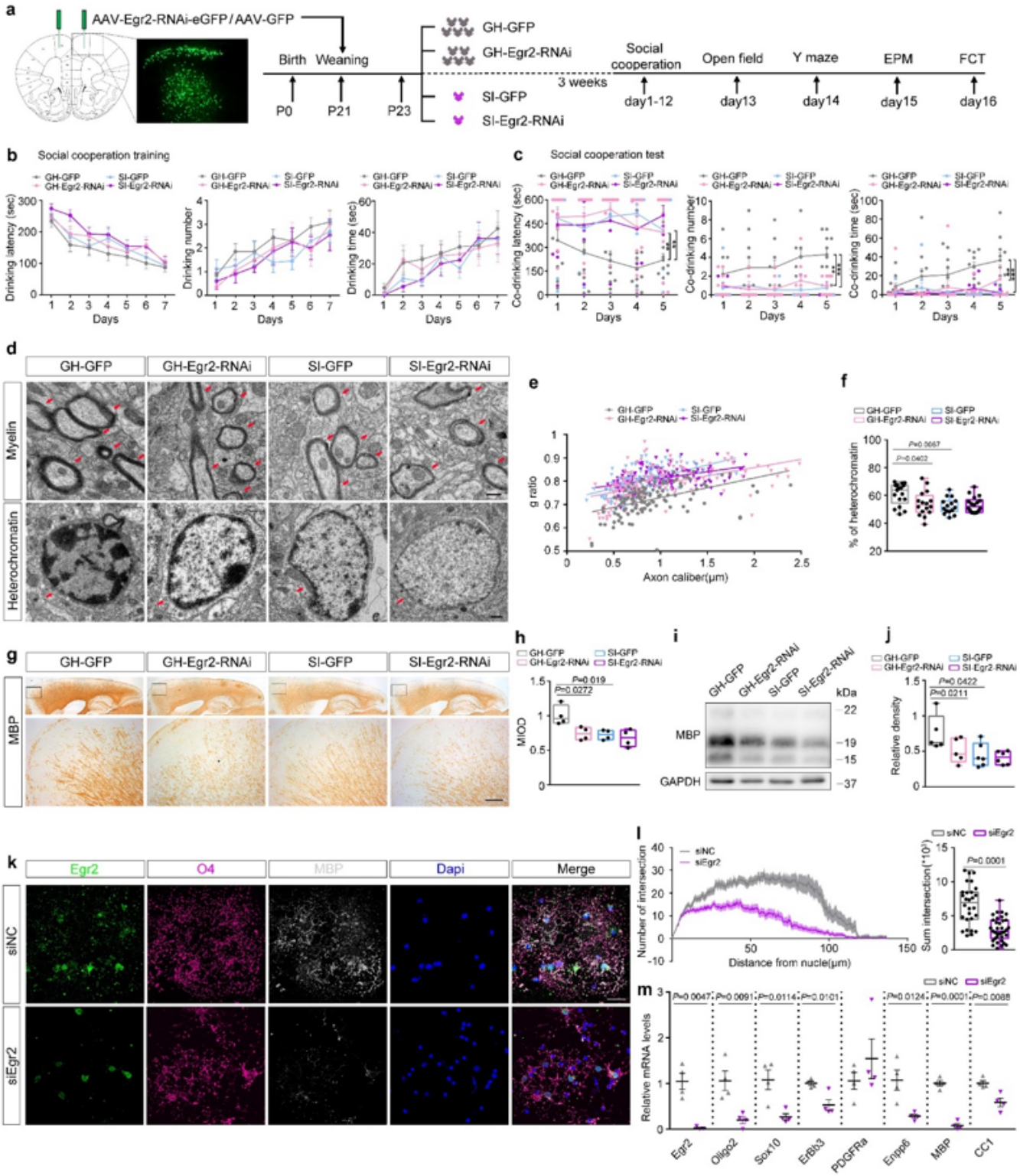


## Figure 3

Knocking down Egr2 led to cooperation defect and myelin impairment. a, A timeline diagram showing mice receiving weanling, AAV virus injection, social isolation, cooperative water-drinking test, and other behavioral tests. b, Graphs showing the time before the first drinking (drinking latency), the times of drinking (drinking number), and the total time spent on drinking (drinking time) each day during the 7 consecutive training days. Note the decline of the drinking latency and the rise of the drinking number

and drinking time. c, Knocking down Egr2 in the mPFC of GH mice decreased the cooperation performance, as assessed by the elevated drinking latency ($F(1, 90) = 11.907$, $P = 0.001$), reduced drinking number ($F(1, 90) = 16.948$, $P = 0.0001$), and reduced drinking time ($F(1, 90) = 9.786$, $P = 0.003$). d, Representative electron microscopy image showing myelin and heterochromatin morphology in the mPFC of GH-GFP, GH-Egr2-RNAi, SI-GFP and SI-Egr2-RNAi mice; red arrows indicate representative myelin or heterochromatin; scale bar, 500 nm. e, Scatter plot of g-ratios with linear least squares fitting in GH-GFP, GH-Egr2-RNAi, SI-GFP and SI-Egr2-RNAi mice; n =128, 139, 116 and 127 axons respectively. Statistical significance was assessed by sum-of-squares F test of the slopes generated by the linear fitting. f, Box plot with dots showing altered percentage of nuclear heterochromatin in GH-GFP, GH-Egr2-RNAi, SI-GFP and SI-Egr2-RNAi mice; n =17, 16, 15 and 18 nuclear respectively. g-j, Representative immunohistology (g) and Western blot (i) images showing MBP expression in GH-GFP, GH-Egr2-RNAi, SI-GFP and SI-Egr2-RNAi mice; h, j, show the respective quantifications. k, Representative immunofluorescence images showing altered differentiation state by knocking down Egr2 in primary oligodendrocytes; scale bar, 50 μm; l, Sholl analysis showing reduced intersections of concentric circles with the oligodendrocyte process reconstructions by knocking down Egr2 in differentiating oligodendrocyte. n = 28 cells for siNC, n = 35 cells for siEgr2. m, qPCR evaluating altered expression of differentiation markers by knocking down in primary oligodendrocytes; Egr2 expression is normalized to GAPDH; O4 and MBP serve as markers for early- and late-differentiated oligodendrocyte, respectively. All data were from 2 months old male C57BL/6 mice. Data in b, c are represented as mean ± SEM from 20 mice per group, and analyzed by repeated-measures ANOVA with post hoc Student-Newman-Keuls test; Data were presented as line plot in b and with dots representing values of each sample in c. Data in f, h, j were analyzed by two-way ANOVA followed by Tukey's post hoc test; n = 4 mice in each group for h and n = 5-6 mice in j. Data were analyzed by two-tailed Student’s t-tests in l and m, n = 3 in m. GH-GFP: GH mice with AAV-GFP virus injection; GH-Egr2-RNAi: GH mice with AAV-Egr2-RNAi virus injection; SI-GFP: SI mice with AAV-GFP virus injection; SI-Egr2-RNAi: SI mice with AAV-Egr2-RNAi virus injection.

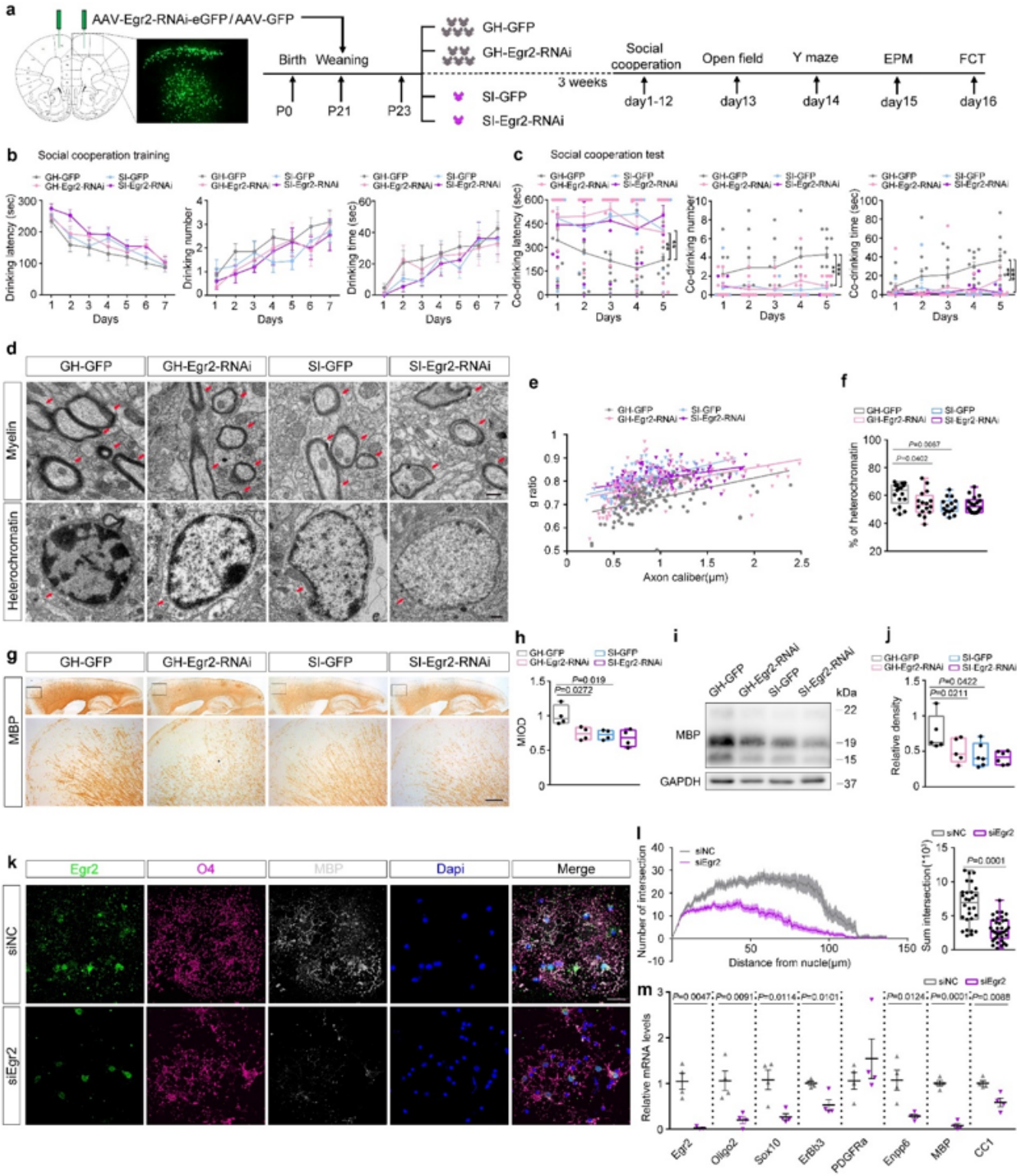


## Figure 3

Knocking down Egr2 led to cooperation defect and myelin impairment. a, A timeline diagram showing mice receiving weanling, AAV virus injection, social isolation, cooperative water-drinking test, and other behavioral tests. b, Graphs showing the time before the first drinking (drinking latency), the times of drinking (drinking number), and the total time spent on drinking (drinking time) each day during the 7 consecutive training days. Note the decline of the drinking latency and the rise of the drinking number

and drinking time. c, Knocking down Egr2 in the mPFC of GH mice decreased the cooperation performance, as assessed by the elevated drinking latency ($F(1, 90) = 11.907$, $P = 0.001$), reduced drinking number ($F(1, 90) = 16.948$, $P = 0.0001$), and reduced drinking time ($F(1, 90) = 9.786$, $P = 0.003$). d, Representative electron microscopy image showing myelin and heterochromatin morphology in the mPFC of GH-GFP, GH-Egr2-RNAi, SI-GFP and SI-Egr2-RNAi mice; red arrows indicate representative myelin or heterochromatin; scale bar, 500 nm. e, Scatter plot of g-ratios with linear least squares fitting in GH-GFP, GH-Egr2-RNAi, SI-GFP and SI-Egr2-RNAi mice; n =128, 139, 116 and 127 axons respectively. Statistical significance was assessed by sum-of-squares F test of the slopes generated by the linear fitting. f, Box plot with dots showing altered percentage of nuclear heterochromatin in GH-GFP, GH-Egr2-RNAi, SI-GFP and SI-Egr2-RNAi mice; n =17, 16, 15 and 18 nuclear respectively. g-j, Representative immunohistology (g) and Western blot (i) images showing MBP expression in GH-GFP, GH-Egr2-RNAi, SI-GFP and SI-Egr2-RNAi mice; h, j, show the respective quantifications. k, Representative immunofluorescence images showing altered differentiation state by knocking down Egr2 in primary oligodendrocytes; scale bar, 50 μm; l, Sholl analysis showing reduced intersections of concentric circles with the oligodendrocyte process reconstructions by knocking down Egr2 in differentiating oligodendrocyte. n = 28 cells for siNC, n = 35 cells for siEgr2. m, qPCR evaluating altered expression of differentiation markers by knocking down in primary oligodendrocytes; Egr2 expression is normalized to GAPDH; O4 and MBP serve as markers for early- and late-differentiated oligodendrocyte, respectively. All data were from 2 months old male C57BL/6 mice. Data in b, c are represented as mean ± SEM from 20 mice per group, and analyzed by repeated-measures ANOVA with post hoc Student-Newman-Keuls test; Data were presented as line plot in b and with dots representing values of each sample in c. Data in f, h, j were analyzed by two-way ANOVA followed by Tukey's post hoc test; n = 4 mice in each group for h and n = 5-6 mice in j. Data were analyzed by two-tailed Student’s t-tests in l and m, n = 3 in m. GH-GFP: GH mice with AAV-GFP virus injection; GH-Egr2-RNAi: GH mice with AAV-Egr2-RNAi virus injection; SI-GFP: SI mice with AAV-GFP virus injection; SI-Egr2-RNAi: SI mice with AAV-Egr2-RNAi virus injection.

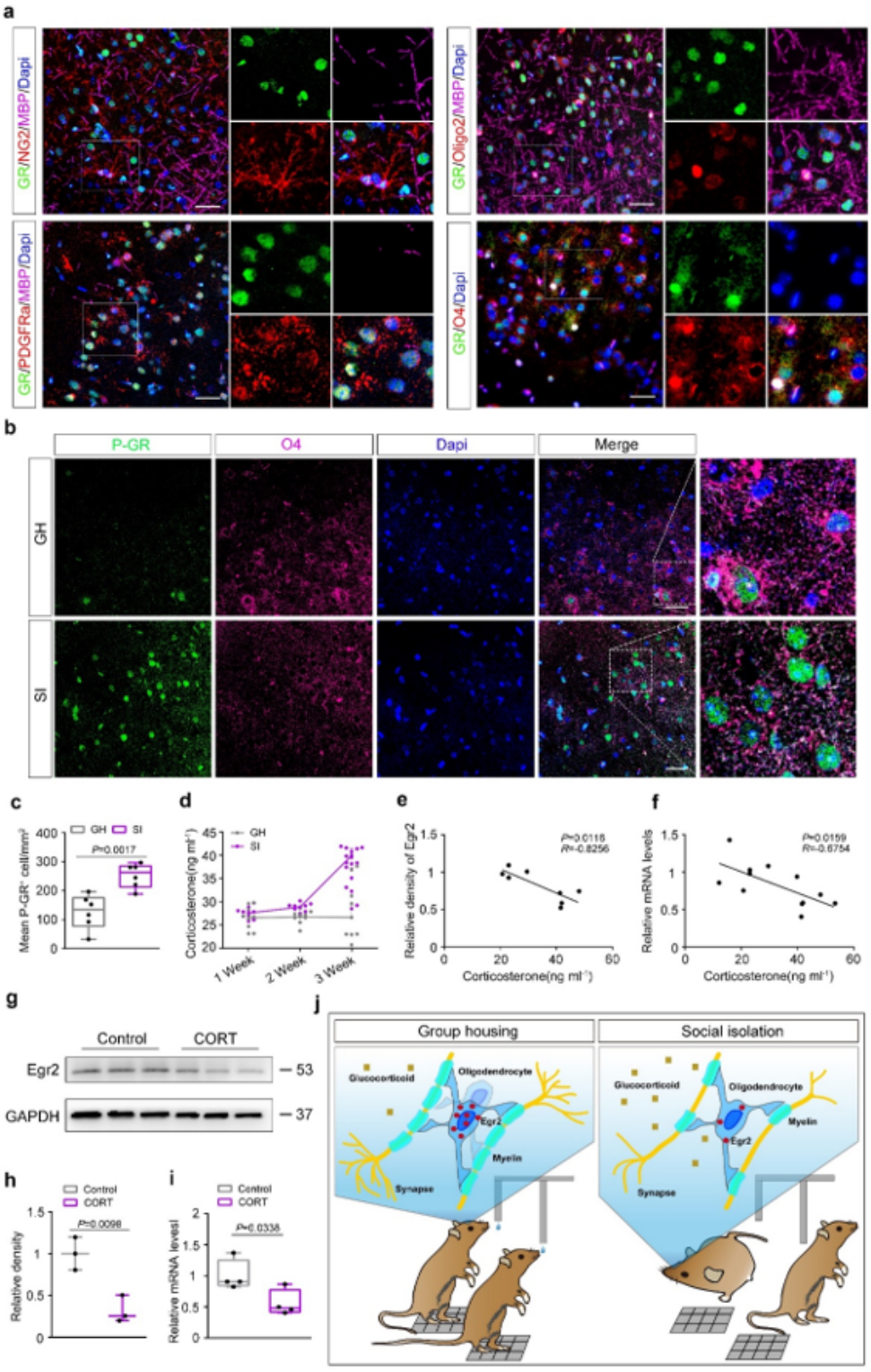


## Figure 4

Regulation of EGR2 by corticosteroid in SI mice. a, Representative immunofluorescence images showing glucocorticoid receptor (GR) expression in the NG2-labeled, Oligo2-labeled, PDGFRα-labeled, O4-labeled and MBP-labeled oligodendrocyte in the mPFC region; scale bar, 50 μm. b, Representative immunofluorescence images showing Phosphorylated GR (pGR) expression in the mPFC of GH and SI mice; scale bar, 50 μm; c, shows the quantified analysis. d, ELISA measurement of corticosteroid levels in

the serum in mice treated by GH or SI for one week, two weeks, and three weeks; GH: n = 9, 9, and 11 mice, respectively; SI: n = 9, 9, and 12 mice, respectively. e, f, Lineal fitting showing negative correlation of serum corticosteroid levels with Egr2 protein (e) or mRNA (f) levels in the mPFC of SI mice. g-i, Representative Western blot images (g) and qPCR analysis (i) showing reduced Egr2 expression after corticosteroid treatment of primary oligodendrocytes; h, shows the quantified analysis of g; EGR2 expression is normalized to GAPDH in g, i. j, Schematic graph showing Egr2 regulate mice's cooperative behavior through modulating oligodendrocyte maturation. Data in a, b are from 2 months old male C57BL/6 mice. All Data were analyzed by two-tailed Student's t-tests and presented as box plot with dots in c, h, g; n = 3 in h, n = 4 in i.

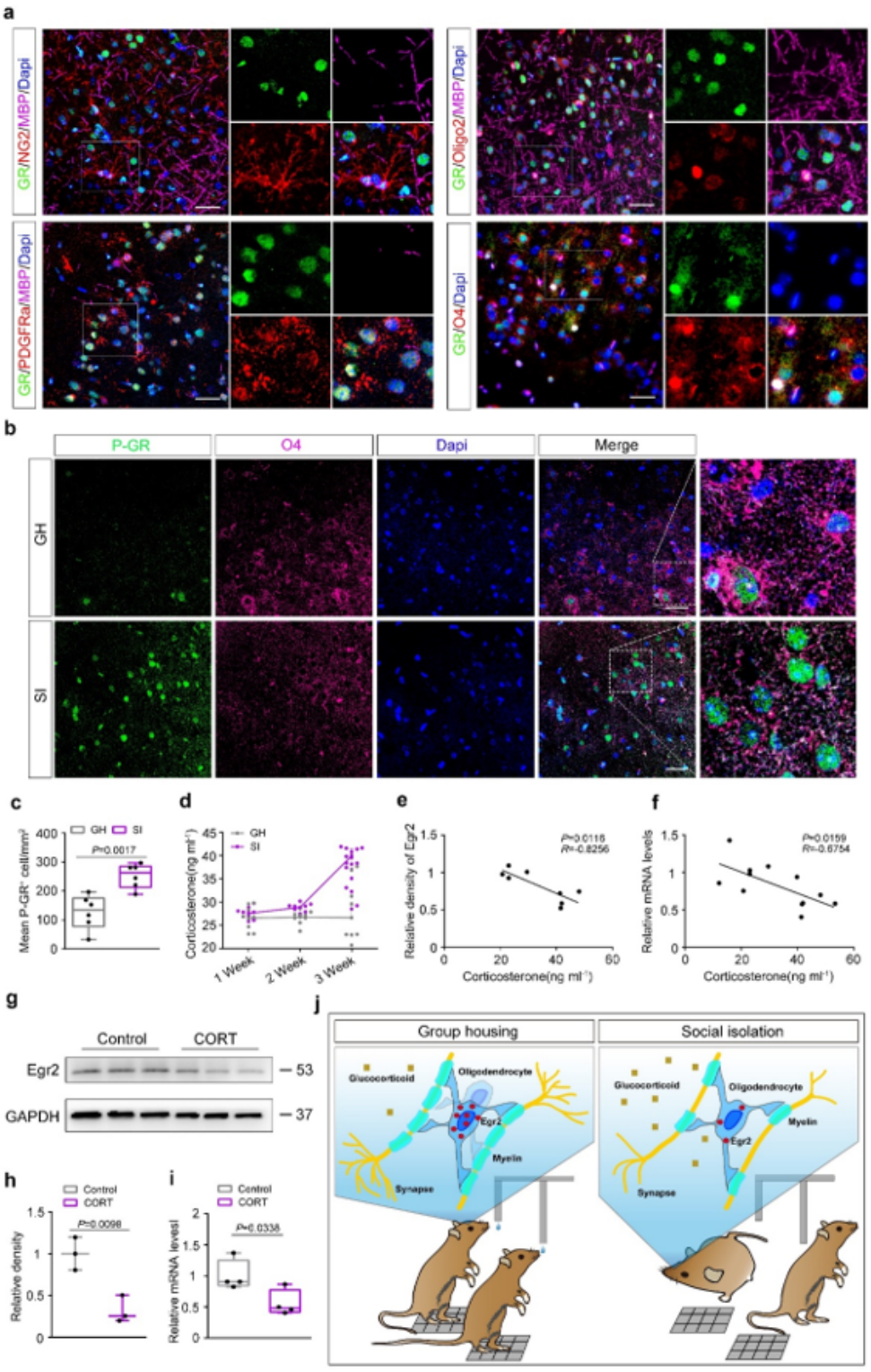


## Figure 4

Regulation of EGR2 by corticosteroid in SI mice. a, Representative immunofluorescence images showing glucocorticoid receptor (GR) expression in the NG2-labeled, Oligo2-labeled, PDGFRα-labeled, O4-labeled and MBP-labeled oligodendrocyte in the mPFC region; scale bar, 50 μm. b, Representative immunofluorescence images showing Phosphorylated GR (pGR) expression in the mPFC of GH and SI mice; scale bar, 50 μm; c, shows the quantified analysis. d, ELISA measurement of corticosteroid levels in

the serum in mice treated by GH or SI for one week, two weeks, and three weeks; GH: n = 9, 9, and 11 mice, respectively; SI: n = 9, 9, and 12 mice, respectively. e, f, Lineal fitting showing negative correlation of serum corticosteroid levels with Egr2 protein (e) or mRNA (f) levels in the mPFC of SI mice. g-i, Representative Western blot images (g) and qPCR analysis (i) showing reduced Egr2 expression after corticosteroid treatment of primary oligodendrocytes; h, shows the quantified analysis of g; EGR2 expression is normalized to GAPDH in g, i. j, Schematic graph showing Egr2 regulate mice's cooperative behavior through modulating oligodendrocyte maturation. Data in a, b are from 2 months old male C57BL/6 mice. All Data were analyzed by two-tailed Student's t-tests and presented as box plot with dots in c, h, g; n = 3 in h, n = 4 in i.

## Supplementary Files

This is a list of supplementary files associated with this preprint. Click to download.

- ExtendedDataFig.andLegends.docx
- ExtendedDataFig.andLegends.docx
- SupplementaryVideo1Socialcooperationtraining.mp4
- SupplementaryVideo1Socialcooperationtraining.mp4
- SupplementaryVideo2Socialcooperationbehavior.mp4
- SupplementaryVideo2Socialcooperationbehavior.mp4
- SupplementaryVideo3Socialuncooperativebehavior.mp4
- SupplementaryVideo3Socialuncooperativebehavior.mp4
- Supplementarytable1qPCRprimers.xlsx
- Supplementarytable1qPCRprimers.xlsx